Exploring the Nature of Wetting by Water of Surfaces of Alkane−Amidethiols Adsorbed on Gold Using the Electrostatic Potential Topology

Yosslen Aray,*,† Jesus Rodríguez,† David Santiago Coll,† Carlos Gonzalez,‡ and Manuel Marquez‡,§,||,⊥

Centro de Quimica IVIC, Apartado 21827, Caracas 1020 A, Venezuela, Physical and Chemical Properties Division, National Institute of Standard and Technologies (NIST), Gaithersburg, Maryland 20899, The Nanotechnology Lab, Kraft Foods R&D, 801 Waukegan Road, Glenview, Illinois 60025, Department of Physics and DEAS, Harvard University, 29 Oxford Street, Cambridge, Massachusetts 02138, and Los Alamos National Laboratory, Chemistry Division, Los Alamos, New Mexico 87545

Received: June 22, 2004; In Final Form: September 15, 2004

The nature of the interaction of water molecules with the surface of a set of experimentally well-studied alkane−amidethiols adsorbed on a gold(111) surface and its effect on the water contact angle have been studied by carrying out a systematic determination of the topology of electrostatic potential using ab initio density functional theory methods for periodic systems. The obtained results have shown that the water contact angle decreases systematically as the number of minima by surface cell unit and the electrostatic potential magnitude at these minima, and consequently the adsorption strength, increases. Thus, this electrostatic potential magnitude can be used as a measure of the efficiency and ability of a chemical group for wetting of a surface by water.

Introduction

Wetting phenomena have long served as a useful means of characterizing surfaces.[1−8] The concept of contact angle is frequently used to characterize the degree of wetting of a surface of a solid by a liquid droplet. This angle, a macroscopic parameter, can be measured accurately from experiments. The shape of the liquid droplet on it essentially characterizes the wetting of a surface. The two extreme shapes are a sphere, where the liquids form a drop on the surface, only partially covering it, the partial wetting state, and a planar film, where the liquid forms a macroscopically thick film covering the solid surface, the complete wetting state. Surface wetting properties are extremely important in many technological applications.[9−16] Over the last few decades, considerable progress has been made in understanding the wetting phenomenon both in the theoretical and experimental fronts.[17−32] Thus, it is well-known that the wetting of a surface is essentially determined by short-range molecular interactions between the liquid and surface atoms close to the solid−liquid interface.[1] These interactions can be divided into dispersion, induction, and polar kinds.[1] Polar interactions, such as electrostatic interactions, hydrogen bonds, and electron acceptor−electron donor interactions, include a lack of symmetry in the charge distribution within the molecules. For highly polar molecules such as water, it should be expected that the polar interactions are the major contributor to the interaction energy with the surface atoms.[1] In the present study, we just focus on the electrostatic contribution, a very important component of the interaction of water with surfaces containing chemical organic groups like $-CH_3$, $-CF_3$, $-NH_2$, $-OH$, $-CN$, and so forth.[1]

The description of the wetting behavior at the microscopic level is relevant to several areas of practical interest such as adhesion, lubrications, foams, wetting of microsized channels,[10] nanopores for the formation of nanowires,[13] and wetting of nanoscale patterned interfaces with application to nanolithography.[16] However, the detailed molecular basis of wetting is still not well understood. The chemical composition role, that is, the nature of the interactions between the drop molecules and the exposed surface atoms and of the surface structure, and the geometry role need to be carefully studied.

The nature of the water−surface interactions can be particularly explored using the electrostatic potential, $V(\mathbf{r})$, which lets us directly determine where the electron-rich sites in a molecule or crystal are localized.[33−40] It is well-known that the topographic features of the electrostatic potential, $V(\mathbf{r})$, are particularly useful for understanding the hydration process.[33−40] In this work, the nature of the interaction of water molecules with the surface of a set of experimentally well-studied[25] alkane−amidethiols adsorbed on a gold(111) surface and its effect on the water contact angle have been studied by carrying out a systematic determination of the topology of $V(\mathbf{r})$ using ab initio density functional theory (DFT) methods for periodic systems. Self-assembled monolayers (SAMs) of $-S[CH_2(C{=}O)NH]-(CH_2)_{11}-CH_3$ (**1**), $-S[CH_2(C{=}O)NH]-CF_3$ (**2**), $-S[CH_2(C{=}O)NH]C_6H_4N(CH_2)_4O$ (**3**), $-S[CH_2(C{=}O)NH](CH_2)_{11}-OH$ (**4**), and $-S[CH_2(C{=}O)NH](CH_2)_{11}-COOH$ (**5**) alkane−amidethiols, whose surfaces contain (**1**)$-CH_3$, (**2**)$-CF_3$, (**3**)$-H_2C-O-CH_2$, (**4**)−OH, and (**5**)−COOH chemical groups, were studied.

Computational Methodology

$V(\mathbf{r})$ at a point, r, generated by a molecule or crystal is given by

* Corresponding author. E-mail: yaray@ivic.ve. Fax: (+58) 212 504 1350.
† Centro de Quimica IVIC.
‡ National Institute of Standard and Technologies (NIST).
§ Kraft Foods R&D.
|| Harvard University.
⊥ Los Alamos National Laboratory.

10.1021/jp047278o CCC: $27.50
Published on Web 11/13/2004

$$V(\mathbf{r}) = V_N(\mathbf{r}) + V_E(\mathbf{r}) \quad (1)$$

where the two terms represent the bare nuclear and electronic contributions, respectively, to the total electrostatic potential. The sign of $V(\mathbf{r})$ at a given point indicates whether the nuclear (positive) or electronic (negative) effects are dominant.

The electrostatic potential at $\mathbf{r}$ generated by the total charge distribution, ρ^{tot}, of a periodic system is given by[41]

$$V(\mathbf{r}) = \sum_n \int \rho^{tot}(\mathbf{r}' - \mathbf{R}_n)|\mathbf{r} - \mathbf{r}'|^{-1}\, d\mathbf{r}' \quad (2)$$

The summation extends to all direct lattice vectors, with the prime on the integral sign indicating that an infinitesimal region about $\mathbf{r} = \mathbf{r}'$ is excluded from the domain of integration to avoid divergent nuclear self-interaction terms that would otherwise arise in the electrostatic energy per cell.[42] ρ^{tot} may be decomposed into electronic and nuclear components

$$\rho^{nuc}(\mathbf{r}) = \sum_a q_a \delta(\mathbf{r}_a, \mathbf{r}) \quad (3)$$

where the summation extends to all the reference cell nuclei, with atomic numbers and position vectors denoted by q_a and $\mathbf{r}_a$, respectively.

$$\rho^{el}(\mathbf{r}) = -\sum_{ij}\sum_{\mu\nu} \mathbf{P}_{\mu\mathbf{R}_i\nu\mathbf{R}_j} \chi_\mu(\mathbf{r} - \mathbf{R}_i)\chi^*_\nu(\mathbf{r} - \mathbf{R}_i) \quad (4)$$

where P is the density matrix and $\chi_\mu(\mathbf{r} - \mathbf{R}_i)$ is the μth reference cell local Gaussian basis function translated by the direct lattice vector $\mathbf{R}_i$. The summation over i and j extends to all direct lattice vectors, while that over μ and ν includes all the basis functions of the reference cell. Substitution of eqs 3 and 4 into eq 2 gives the nuclear and electronic $V(r)$ contributions.

The topological properties of $V(\mathbf{r})$ are summarized by its critical points (CPs). These are points where the gradient vector field, $\nabla V(\mathbf{r})$, vanishes, and they are classified by the $V(\mathbf{r})$ curvatures or three eigenvalues, λ_i (i = 1, 2, or 3), of the corresponding Hessian matrix ($H_{ij} = \partial^2 V(\mathbf{r})/\partial x_i \partial x_j$). In molecules and crystals, there can be four types of these extremes that are labeled by their rank (number of nonzero eigenvalues) and signatures (excess number of positive over negative eigenvalues). These can be maxima (3, −3), minima (3, +3), or (3, −1) and (3, +1) saddles that bridge either two minima or two maxima. For the region nearest to the nucleus, V_N dominates and $V(\mathbf{r})$ has a similar topology to that of the electron density,[43] $\rho(r)$, that is, positive-valued maxima at the nuclear site and a positive-valued (3, −1) bond saddle between every pair of bonded atoms. Nevertheless, the existence of a maxima is ruled out via an established result that, barring the nuclear position, any strict local maxima in the $V(\mathbf{r})$ map cannot exist.[36] However, a (3, −1) CP corresponding to a bond saddle point between each pair of atoms still remains. For the region where V_E dominates ($V(\mathbf{r})$ is negative), the $V(\mathbf{r})$ topography can be more complex. However, it is well-known that lone pairs of electrons as well as double π-bonds (C═C, C═N, etc.) are generally characterized as negative-valued minima.[35,36] In summary, the region nearest to the nucleus is always positive-valued, while the region where the potential is negative-valued contains the minima that characterized the atom lone pairs. The set of CPs of a molecule are unique, and hence, their existence and nature offer a signature of the structure of the molecule.[35,36] The main topographic features of $V(\mathbf{r})$ are easily visualized using three-dimensional (3D) maps of isovalued contours. In these maps, the minima show their distinctive topological features: equi-potential contours that become more and more closest to the minimum as the absolute magnitude of the isosurface value is increased toward the $V(\mathbf{r})$ value at the minimum. Figure 1 shows the $V(\mathbf{r})$ topological features of an isolated water molecule. The negative potential (blue, yellow, and green isosurfaces) is located over the nonbonding region of the oxygen atom, forming a lone pair pattern like *rabbit ears* with two negative-valued minima (red spheres) connected by a (3, +1) saddle point. The $V(\mathbf{r})$ over the entire nuclear region is positive (brown zone), with a saddle CP associated to each OH bond. By locating CPs in substrate electrostatic potentials, one can precisely identify the host sites in which water molecules should bind. Maintaining complementary between the $V(\mathbf{r})$ features of substrate and water, the positive-valued $V(\mathbf{r})$ zone of the hydrogen atoms in the water molecules are positioned over the minima of the negative $V(\mathbf{r})$ zone of the substrate. Additionally, the $V(\mathbf{r})$ topology-based theory predicts that the attractive interactions $(OH)_{water} \rightarrow (\text{negative minima})_{substrate}$ will be stronger as the absolute value of $V(\mathbf{r})$ at the minima increases.[33−36,44]

Figure 1. Contour maps of the electrostatic potential for the H_2O molecule. The blue, yellow, and green zones denote negative values of $V(r)$, while the brown zone denotes the positive one. The red spheres denote the $V(r)$ minima critical points characterizing the oxygen lone pairs, and the red and white cylinders denote the oxygen and hydrogen atoms.

The topology of $V(\mathbf{r})$ was analyzed using an algorithm developed in our laboratory, in the same way to those developed for the study of the electronic density topology.[45]

The CPs were calculated using the Newton−Raphson (NR) technique.[46] The NR algorithm starts from a truncated Taylor expansion at the point $\mathbf{r} = \mathbf{r}_0 + \mathbf{h}$ about $\mathbf{r}_0$ of a multidimensional scalar function ($\nabla V(\mathbf{r})$):

$$\nabla V(\mathbf{r}) = \nabla V(\mathbf{r}_0) + \mathbf{H}_0\mathbf{h} + \text{higher-order terms} \quad (5)$$

where $\mathbf{H}$ is the Hessian (the Jacobian of $\nabla V(\mathbf{r})$) at point $\mathbf{r}_0$. Given that a CP is characterized by $\nabla V(\mathbf{r}) = 0$, the optimal step, $\mathbf{h}$, is then given by $\mathbf{h} = -\mathbf{H}^{-1}\nabla V(\mathbf{r}_0)$. This second-order correction is then used to obtain the vector $\mathbf{r}_{new} = \mathbf{r}_{old} + t\mathbf{h}$ (t is a small value), and the process is iterated to $\nabla V(\mathbf{r}) = 0$. The NR algorithm requires the evaluation of the first V' and second V'' partial derivatives of $V(\mathbf{r})$, at arbitrary points, $\mathbf{r}$. These partial derivatives are evaluated by numerical differences and are fed into an automated algorithm for the systematic determination of all the CPs inside the unit cell of the crystal.

$V(\mathbf{r})$ was calculated by means of the Dmol^3 [47, 48] program using the Kohn−Sham Hamiltonian with the gradient-corrected Perdew−Becke−Ernzerhof (PBE) exchange-correlation functional.[49] Dmol^3 calculates variational self-consistent solutions to the DFT equations, expressed in a numerical atomic orbital

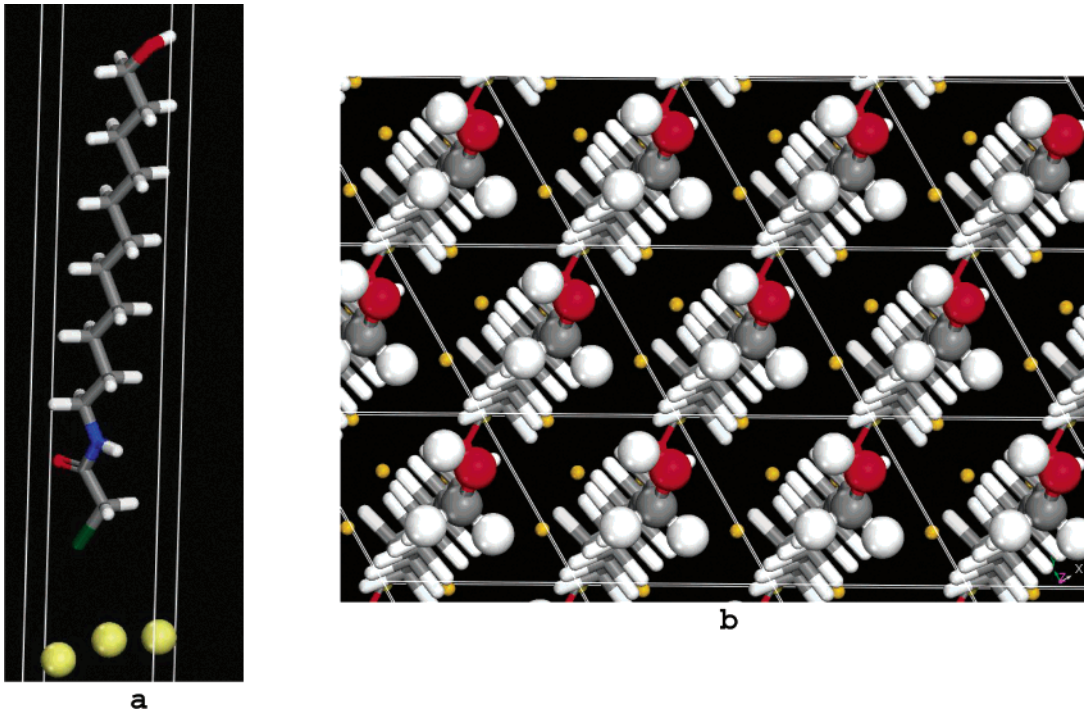

Figure 2. (a) Side view of a cylinder model of the SAM unit cell (white lines) of **4**(−OH) adsorbed on the Au(111) surface. The green, red, blue, gray, and white cylinders denote the sulfur, oxygen, nitrogen, carbon, and hydrogen atoms, respectively. The yellow spheres denote the gold atoms of the top layer of the Au(111) surface. (b) Top view showing the packing of the surface and highlighting the exposed $-CH_2OH$ group whose hydrogen, carbon, and oxygen atoms are denoted as white, gray, and red spheres, respectively.

basis. The solutions to these equations provide the molecular electron densities, which can be used to evaluate the total electrostatic potential of the system. The numerical double-ζ plus polarization basis set *DNP*[47] was used in all calculations.

Surface Models

At full coverage, the SAM structure of the alkanethiols is highly ordered, with the following basic structural model proposed: the hexagonal $(\sqrt{3} \times \sqrt{3})R30°$ lattice which contains just one molecule per three gold surface atoms.[50,51] This model leads to a closely packed structure containing molecules packed in the same orientation. A c(4×2) super lattice of the hexagonal one containing four molecules with two inequivalent chains per cell packed in two orientations, where alkanethiols can form sulfur headgroup dimers with a S−S spacing of 2.2 Å, is also possible.[50,51] The amide group of the alkane−amidethiols in the headgroup region gives rise to intermolecular NH···O=C hydrogen bonding between adjacent molecules which can control the conformation of the SAMs. It is known that this lateral hydrogen bonding stabilizes the all-trans conformation of the amino moiety with a S−S spacing of 5.1 Å.[25] For this reason and for simplicity of discussion, we have chosen the $(\sqrt{3} \times \sqrt{3})R30°$ lattice as the SAM model. The metallic surfaces were modeled by cells containing a periodic slab of six layers of gold atoms initially having the same structure as the (111) surface of the gold bulk. The choice of this slab size is based on reported tests, which have shown converged energy calculations with an error of ∼0.01 eV.[50] Vacuum layers thicker than 15 Å were used to ensure that there were no interactions between adjacent slabs. Figure 2 shows an example of this surface model for the SAM of the **4**(−OH) alkane−amidethiol.

The structure (geometry and cell parameters) of these SAMs was optimized using algorithms contained in the Castep program.[52] In this program, the Kohn−Sham equations of DFT

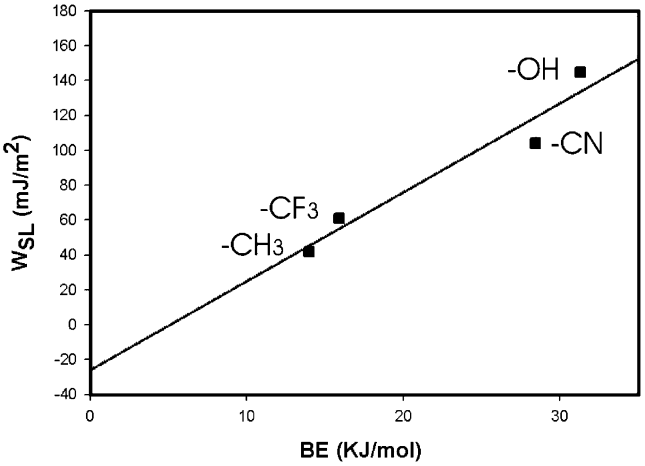

Figure 3. Experimental work of adhesion values, W_{SL}, plotted versus the calculated binding energy, BE, of monolayers of water molecules on SAM surfaces that expose $-CH_3$, CF_3, −OH, and −CN groups.

TABLE 1: Optimized Lattice Parameters and Intermolecular NH···O=C Bond Lengths for the Studied SAMs

SAM	*a* (Å)	*b* (Å)	*c* (Å)	α (Å)	*β* (Å)	*γ* (Å)	$r_{NH\cdots OC}$ (Å)
1	4.782	4.967	30.000	90.2	88.3	119.3	1.955
2	4.962	4.934	30.023	89.4	90.9	121.0	1.996
3	5.108	5.134	30.447	90.1	89.2	115.8	2.346
4	4.897	4.973	29.990	89.7	89.6	119.4	2.073
5	4.765	5.042	29.907	90.1	88.5	119.2	2.010

are variationally solved in a plane-wave basis set using optimized ultrasoft pseudopotentials in Kleinman−Bylander form[53] for the description of the electron−ion interactions. The exchange-correlation part of the Hamiltonian is described using the generalized gradient approximation of Perdew, Burke, and Ernzerhof.[49] A conjugate gradient minimization scheme is utilized to locate the electronic ground states directly. The

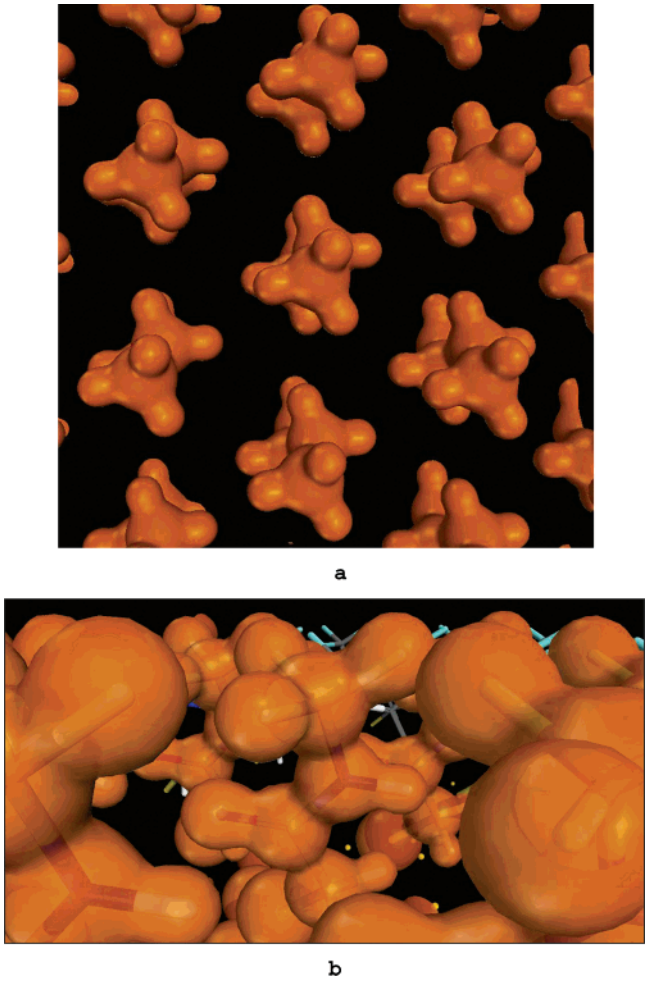

Figure 4. (a) Top and (b) side views of the 3D contour map of $V(\mathbf{r})$ for the **1**($-CH_3$) surface. The brown zones denote positive values of $V(\mathbf{r})$.

calculation of the Hellmann−Feynman forces acting on the atoms and a standard BFGS technique allows the structural optimization. In contrast to Dmol[3], the Castep program allows us to optimize the cell parameters. The obtained parameters are reported in Table 1. The results show that, in general, a modest change (from $a = b = 4.95$ Å, $\alpha = \beta = 90°$, and $\gamma = 120°$ for the gold bulk) of the lattice constants a, b, α, β, and γ has been obtained. The molecules are tilted and participating in NH···O═C intermolecular hydrogen bonds whose lengths are also reported in Table 1. Unfortunately, manipulation and handling of $V(\boldsymbol{r})$ are hard to do using Castep. Additionally, this software contains a pseudopotential method in which the electron core contribution to $V(\boldsymbol{r})$ is discarded, and it is well-known[54,55] that this contribution is important to obtain the right magnitude of the topological properties of fields such as as the electronic density, its Laplacian, or $V(\boldsymbol{r})$. Therefore, we have used Castep to optimize the structure of the SAMs and Dmol[3] (a full electron method) to determine the topology of $V(\boldsymbol{r})$ for the optimized structures.

Results and Discussion

The Young−Dupre equation[56,57]

$$W_{SL} = \gamma_L(1 + \cos\theta) \tag{6}$$

relates the contact angle to the work of adhesion, W_{SL}, between the solid and liquid. W_{SL} is the free energy change, or reversible work, of separating unit areas of liquid and solid phases and is given by

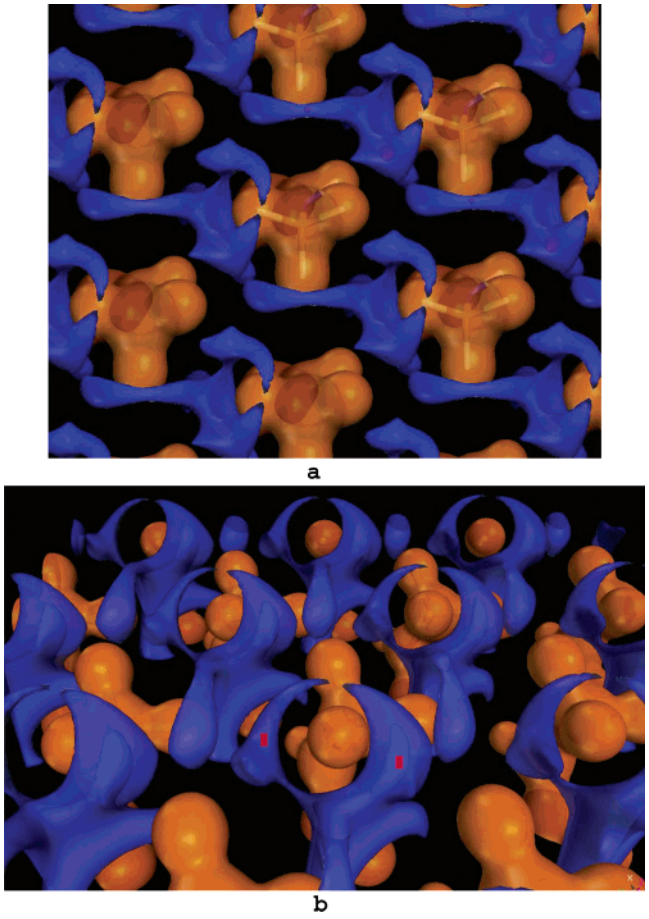

Figure 5. (a) Top and (b) side views of the 3D contour map of $V(\mathbf{r})$ for the **2**($-CF_3$) surface. The brown zones denote positive values of $V(\mathbf{r})$, while the blue zones denote the negative values of the potential.

$$W_{SL} = (\gamma_S + \gamma_L) - \gamma_{SL} \tag{7}$$

where γ_S, γ_L, and γ_{SL} are the solid surface energy, the liquid surface tension, and the interfacial energy or interfacial tension, respectively. From eq 6, W_{SL} can be determined from the two measurable quantities θ and γ_L. For water, γ_L is equal to 72.4 mJ/m^2.[20] Water−surface adhesion should be related to the adsorption strength of a network of chemisorbed or physisorbed water molecules onto the interface.[1,58−59] Therefore, we have estimated the *HOH···surface* binding energy (BE) for **1**($-CH_3$, $\theta = 117°$), **2**($-CF_3$, $\theta = 99°$), and **4**($-OH$, $\theta = 20°$), placing a monolayer of water molecules (one per cell) inside the surface cell, and the system was completely optimized while the cell parameters were fixed. In view of the fact that θ values of SAMs of thiols containing the amide moiety are comparable to those of alkanethiols with the same backbone structure,[25] we have also determined the BE for a SAM of $-S(CH_2)_8-CN$ whose surface contains the $-CN$ group ($\theta = 64$).[24b] BE was calculated by the following expression:

$$BE = E_{S-W} - E_S - E_W \tag{8}$$

where E_{S-W} = total energy of the H_2O monolayer adsorbed on the surface, E_S = total energy of the isolated surface, and E_W = total energy of the H_2O layer isolated in the cell.[60] Figure 3 shows the experimental W_{SL} values as a function of the calculated BE values. The adhesion and BE show a linear

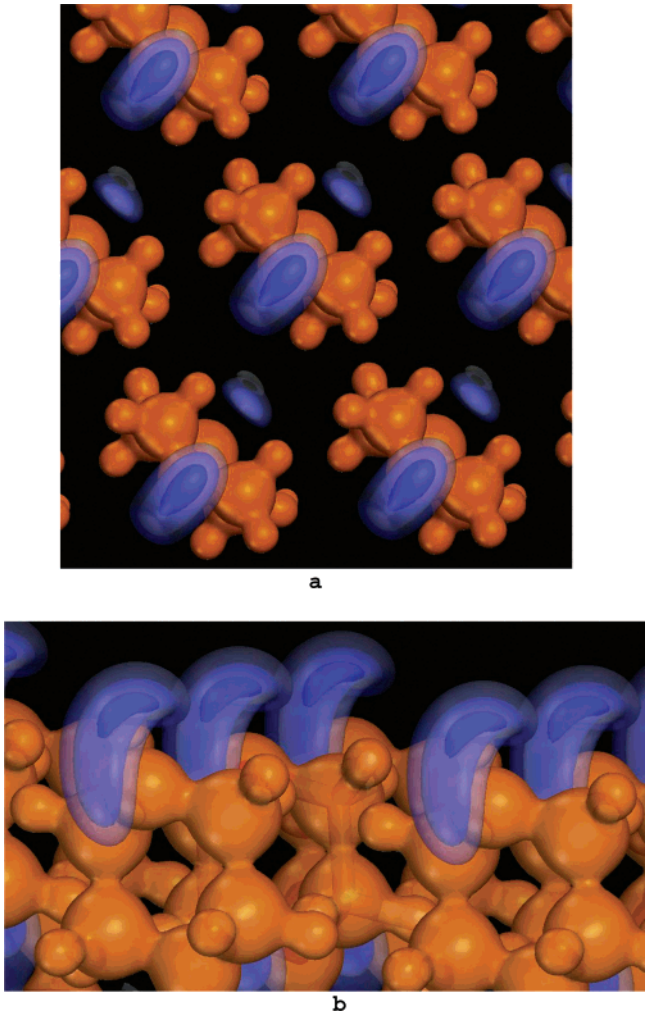

Figure 6. (a) Top and (b) side views of the 3D contour map of $V(\mathbf{r})$ for the **3**(−COC−) surface. The brown zones denote positive values of $V(\mathbf{r})$, while the blue zones denote the negative values of the potential.

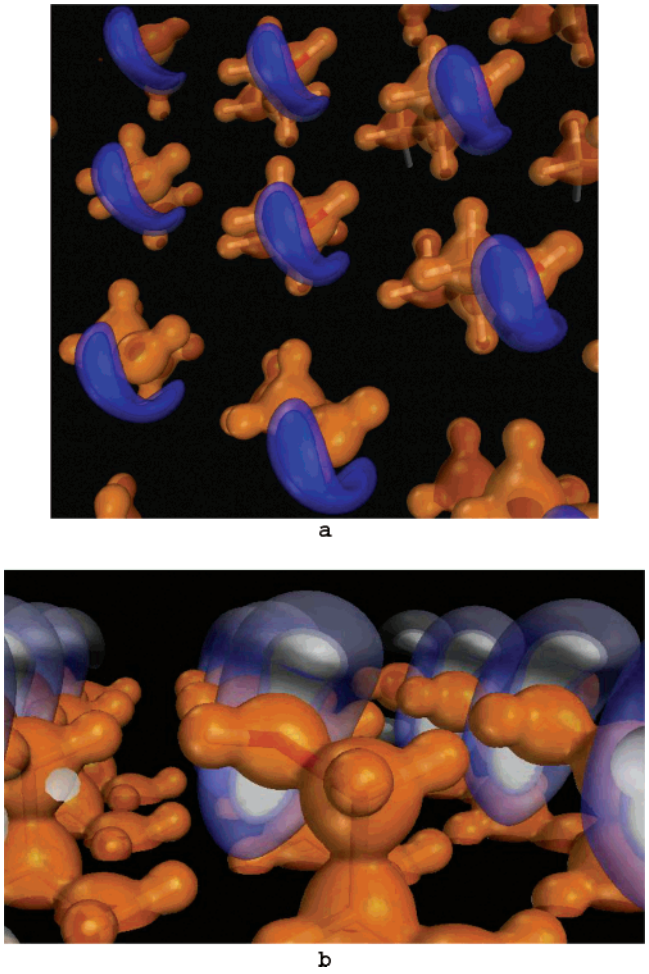

Figure 7. (a) Top and (b) side views of the 3D contour map of $V(\mathbf{r})$ for the **4**(−OH) surface. The brown zones denote positive values of $V(\mathbf{r})$, while the blue and white zones denote the negative values of the potential.

correlation, suggesting that the interfacial bonding is dominated by the strength of local chemical bonds between the hydrogen atoms of the first layer of water molecules and the outermost atoms of the surface.

In general, this kind of bond is strongly electrostatic in nature[1,61−62] and, consequently, $V(\mathbf{r})$ topology offers a powerful tool for understanding the nature of these local *HOH*• • •*surface* bonds. Figures 4−8 display calculated 3D maps showing the main topological features of $V(\mathbf{r})$ for the studied systems, and Table 2 reports the major topological properties (curvatures, λ_i, and the values of $V(\mathbf{r})$ at the CP sites) for the CPs exhibited in the first layers of water molecules. As expected, $V(\mathbf{r})$ is positive (light brown zone) over the entire nuclear region with a saddle CP for each bond in this zone. For **1**(−CH_3), this zone surrounds all of the hydrophobic aliphatic chain and, therefore, the surface exposes a positive zone to the water molecules. For **3**(−COC−), **4**(−OH), and **5**(−COOH), a negative region (blue zone) was localized outside the surface over the nonbonding region of the outermost oxygen atoms each containing a (two for −COOH) nonbonded minimum CP. For **4**(−OH) and **5**(−COOH), the exposed negative lone pairs hinder free access to the positive area of the surface. For **2**(−CF_3), a set of minima around the top fluorine atoms and located inside the surface was found. A saddle point enjoying the exposed ending zone of each pair of fluorine minimum was also determined. It is clear that **3**(−COC−), **4**(−OH), and **5**(−COOH) expose oxygen minima lone pairs (they are above the surface) to the incoming water molecules, while 2(−CF_3) exposes the ending zone of the banana minimum. Therefore, the hydrogen atoms (positive zone) of the water molecules mainly interact with the negative oxygen minima (point of maximum attraction) at the top of the surface of **3**, **4**, and **5**, while on **1** they interact with an electron-poor region.

The topology of $V(\mathbf{r})$ predicts attractive interactions of water molecules on surfaces of **3**, **4**, and **5** with adsorption modes involving attractive interactions between the positive zone around the hydrogen atoms of the water molecules and the negative minima lone pairs at the oxygen atoms of the surfaces. Two active points for adsorption and bigger $V(\mathbf{r})$ values (see Table 2) at these points predict a stronger adsorption mode on **5**(−COOH). The topology-based theory also predicts[33−36,44] that these attractive interactions will be stronger as the values of $V(r)$ at the negative minima, V(CPs), are deeper. Thus, from Table 2, the trend of adsorption strength for the first layer of water molecules that we should expect is **5**(−COOH) > **4**(−OH) > **3**(−COC−) > **2**(−CF_3) ≫ **1**(−CH_3), and this is exactly the same trend of W_{SL}: −COOH (W_{SL} = 141.995 mJ/m^2) > −OH (W_{SL} = 140.434) > −COC (W_{SL} = 109.689) > −CF3 (W_{SL} = 61.074) > −CH3 (W_{SL} = 39.531). Correspondingly, this sequence has the inverse trend for the measured contact angle, −COOH (θ = 16°) < −OH (θ = 20°) < −COC (θ = 59°) < −CF3 (θ = 99°) < −CH3 (θ = 117°). Given that the contact angle of monolayers prepared from thiols

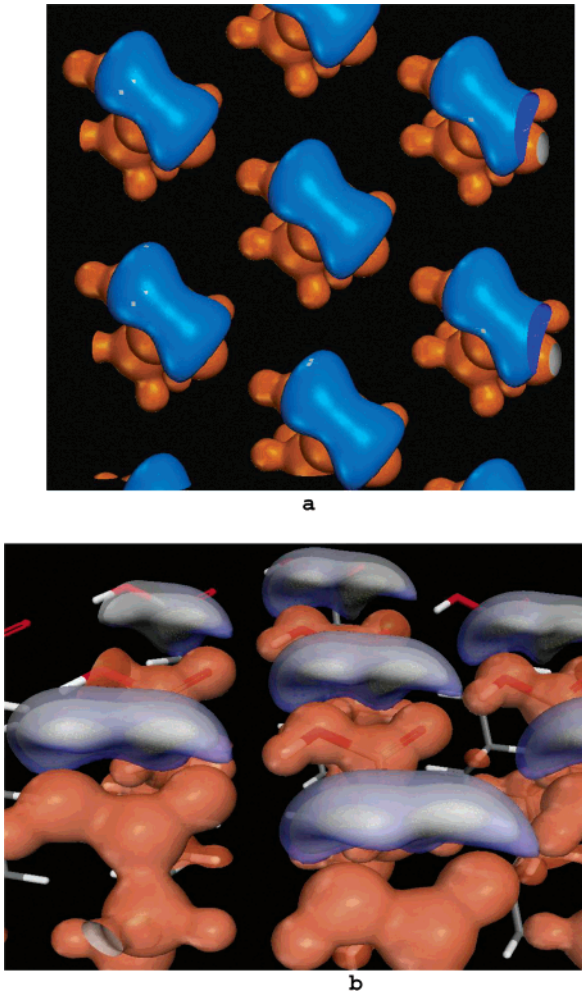

Figure 8. (a) Top and (b) side views of the 3D contour map of $V(\mathbf{r})$ for the **5**(−COOH) surface. The brown zones denote positive values of $V(\mathbf{r})$, while the blue and white zones denote the negative values of the potential.

TABLE 2: Topological Properties (Curvatures, λ_i, and $V(r)$ Values at the CP Sites, V(CPs), in Atomic Units) of $V(r)$ at the Critical Point Exposed by the Surfaces

Negative Region					
	exposed CP	λ_1	λ_2	λ_3	V(CPs)
2(−CF3)	F saddle	−0.0011	0.0101	0.0360	−0.0381
3(−COC−)	−O− minimum	0.0080	0.0299	0.1464	−0.0459
4(−OH)	HO minimum	0.0099	0.0327	0.1823	−0.0509
5(−COOH)	CO minimum	0.0128	0.0265	0.1234	−0.0521
	HO minimum	0.0048	0.0162	0.1015	−0.0460
Positive Region					
	exposed saddle CP	λ_1	λ_2	λ_3	V(CPs)
1(−CH3)	H−C	−2.5470	−2.5320	8.4570	0.8300
2(−CF3)	F−C	−2.1800	−2.1750	8.8470	1.0020
3(−COC−)	C−O	−1.7760	−1.6310	7.7250	0.8460
	H−C	−2.4510	−2.4040	8.2800	0.8670
4(−OH)	H−O	−4.2630	−4.0950	13.8370	1.1060
	C−O	−1.6530	−1.5250	6.8750	0.7630
	H−C	−2.4600	−2.4190	8.5080	0.8120
5(−COOH)	H−O	−3.8541	−3.7689	12.3292	1.0980
	C−O	−2.2485	−2.1384	9.17250	1.0256
	C−C	−1.1733	−1.1511	5.62020	0.7489
	H−C	−2.4742	−2.4512	8.45470	0.8211

containing the amide moiety are comparable to those prepared from alkanethiols with the same backbone structure,[25] we have also determined the negative lone pair CPs for SAMs of $-S(CH_2)_{17}CH{=}CH_2$ (θ = 107)[24b] and $-S(CH_2)_8-CN$ (θ = 64).[24b] A minima lone pair about the carbon double bond with a V(CPs) value of −0.025 au and a minima one for the nitrogen atom of the CN group with a V(CPs) value of −0.048 au were found. A well adjustment of these parameters to the above trends can be observed. Figure 9 plots the experimental W_{SL} values as a function of V(CPs) and shows that the adhesion exponentially increases with increasing V(CPs). Therefore, this result shows that θ decreases systematically as the number of minima by cell unit and V(CPs) on the surface, and consequently the adsorption strength, increases. Thus, V(CPs) can be used as a measure of the efficiency and ability of a chemical group for wetting of a surface by water.

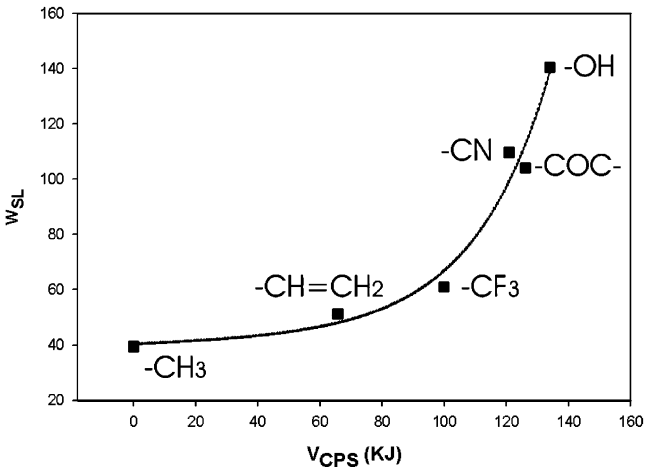

Figure 9. Experimental adhesion, W_{SL} (mJ/m^2), as a function of the value of the electrostatic potential at the exposed critical points, V_{CPs} (kJ).

Finally, the $V(\mathbf{r})$ topology-based theory confirms that there is a strong relationship between the macroscopic contact angle and the adsorption strength of the water molecules just bonded at the interface, that is, the closest adsorbed water monolayer at the surface. Additionally, it is important to remark that the present study just focuses on the electrostatic contribution to the *HOH···surface* bonds. Hydrogen bonding is another factor that can affect the *HOH···surface* interaction, and a correlation between the topological properties of the CPs of the charge density Laplacian with the strengths of these kinds of bonds has been previously reported.[63] We have done a similar study, and the results will be reported in a future publication.

References and Notes

(1) Israelachvili, J. Intermolecular and Surfaces Forces; Academic: London, 1985.
(2) Hugh, D. B. *Adv. Colloid Interface Sci.* **1980**, *14*, 3−41.
(3) Bain, C. D.; Whitesides, G. M. *J. Am. Chem. Soc.* **1988**, *110*, 5897−5898.
(4) Blossey, R. *Nat. Mater.* **2003**, *2*, 301.
(5) Mittal, K. L., Ed. *Contact Angle, Wettability and Adhesion*: VSP: Utrecht, The Netherlands, 1993.
(6) Fowkes, F. M., Ed. *Contact Angles, Wettability and Adhesion*; Advances in Chemistry 43; American Chemical Society: Washington, DC, 1964.
(7) Adamson, A. W. *Physical Chemistry of Surfaces*, 5th ed.; Wiley: New York, 1982.
(8) Zisman, W. In *Contact Angles, Wettability and Adhesion*; Fowkes, F. M., Ed.; Advances in Chemistry 43; American Chemical Society: Washington, DC, 1964; pp 1−51.
(9) Heath, J. R.; Knobler, C. M.; Leff, D. V. *J. Phys. Chem. B* **1997**, *101*, 189.
(10) Lipowsky, R. *Curr. Opin. Colloid Interface Sci.* **2001**, *6*, 40.
(11) Weigl, B. H.; Yager, P. *Science* **1999**, *283*, 346.
(12) Kopp, M. U.; de Mello, A. J.; Manz, A. *Science* **1998**, *280*, 1046.
(13) Ajaya, P. M.; Iijima, S. *Nature (London)*, **1993**, *361*, 333.

(14) Gunze, M. *Science* **1999**, *283*, 41.
(15) Blokhuis, E. M.; Widom, B. *Curr. Opin. Colloid Interface Sci*. **1996**, *1*, 424.
(16) Swain, P. S.; Lipowsky, R. *Langmuir* **1998**, *14*, 6772.
(17) Wu, S. *Polymer Interface and Adhesion*; Marcel Dekker: New York, 1982.
(18) de Genes, P. G. *Rev. Mod. Phys*. **1985**, *57*, 827.
(19) Sharma, P. K.; Hanumantha Rao, K. *Adv. Colloid Interface Sci*. **2002**, *98*, 341.
(20) Colorado, R., Jr.; Randall Lee, T. *J. Phys. Org. Chem.* **2000**, *13*, 796.
(21) Zisman, W. A.; Shafrin, E. G. *J. Phys. Chem*. **1962**, *66*, 740.
(22) Atre, S. V.; Liedberg, B.; Allara, D. L. *Langmuir* **1995**, *11*, 3882.
(23) Troughton, E. B.; Bain, C. D.; Whitesides, G. M.; Nuzzo, R. G.; Allara, D. L.; Porter, M. D. *Langmuir* **1988**, *4*, 365.
(24) (a) Bain, C. D.; Whitesides, G. M. *Science (Washington, D.C.)* **1988**, *240*, 62. (b) Bain, C. D.; Truoghton, E. B.; Tao, Y.-T.; Evall, J.; Whitesides, G. M.; Nuzzo, R. G. *J. Am. Chem. Soc*. **1989**, *111*, 321.
(25) Tam-Chang, S.-W.; Biebuyck, H. A.; Whitesides, G. M.; Jeon, N.; Nuzzo, R. G. *Langmuir* **1995**, *11*, 4371.
(26) Miura, Y. F.; Takenaga, M.; Koini, T.; Graupe, M.; Garg, N.; Graham, R. L., Jr.; Randall Lee, T. *Langmuir* **1998**, *14*, 5821.
(27) Kang, J. F.; Jordan, R.; Ulman, A. *Langmuir* **1998**, *14*, 3983.
(28) Fan, C. F.; Cagin T. *J. Chem. Phys*. **1995**, *103*, 9053.
(29) Hautman, J.; Klein, M. L. *Phys. Rev. Lett.* **1991**, *67*, 1763.
(30) Powell, C.; Fenwick, F.; Bresme, F.; Quirke, N. *Colloids Surf., A* **2002**, *206*, 241.
(31) Bresme, F.; Quirke, N. *PCCP* **1999**, *1*, 2149. Tang, J. Z.; Harris, J. G. *J. Chem. Phys*. **1995**, *103*, 8201.
(32) Gadre, S. R.; Babu, K.; Rendell, A. P. *J. Phys. Chem. A* **2000**, *104*, 8976.
(33) Leboeuf, M.; Koster, M.; Jug, K.; Salahub, D. R. *J. Chem. Phys*. **1999**, *111*, 4893.
(34) Gadre, S. R.; Shirsat, R. N. *Electrostatics of Atoms and Molecules* (an educational monograph); Universities Press: Hyderabad, India, 2000.
(35) Pingale, S. S.; Gadre, S. R.; Bartoli, L. J. *J. Phys. Chem. A* **1998**, *102*, 9987.
(36) (a) Gadre, S. R.; Kulkarni, S. A.; Shivastava, I. A. *J. Chem. Phys*. **1992**, *96*, 5253. (b) Gadre, S. R.; Pathak, R. K. *Proc.—Indian Acad. Sci., Chem. Sci*. **1989**, *102*, 18.
(37) Alhambra, C.; Luque, F. J.; Orozco, M. *J. Phys. Chem.* **1995**, *99*, 3084.
(38) Politzer, P., Truhlar, D. G., Eds. *Chemical Applications of Atomic and Molecular Electrostatic Potentials*; Plenum: New York, 1982.
(39) Murray, J. S., Sen, K. D., Eds. *Molecular Electrostatic Potential: Concepts and Applications*; Elsevier: Amsterdam, The Netherlands, 1996.
(40) Orozco, M.; Luque, F. J. *Theor. Comput. Chem.* **1996**, *3*, 181.
(41) Saunders, V. R.; Freyria-Fava, C.; Dovesi, R.; Salasco, L.; Roetti, C. *Mol. Phys.* **1992**, *77*, 629.
(42) Dovesi, R. *Phys. Status Solidi* **2000**, *217*, 63.
(43) Keith, T. A.; Bader, R. F. W.; Aray, Y. *Int. J. Quantum Chem*. **1996**, *57*, 183.
(44) Aray, Y.; Marquez, M.; Rodríguez, J.; Coll, S.; Simón-Manso, Y.; Gonzalez, C.; Weitz, D. A. *J. Phys. Chem. B* **2003**, *107*, 8946.
(45) Aray, Y.; Rodríguez, J.; Vega, D. *Comput. Phys. Commun.* **2002**, *143*, 199.
(46) *Numerical Recipes in Fortran 77: The Art of Scientific Computing*; Cambridge University Press: 1992; p 708.
(47) *DMol*^{3}; available as part of Material Studio; Accelrys Inc.: San Diego, CA, 2002.
(48) Delley, B. *J. Chem. Phys*. **1990**, *92*, 508; **2000**, *113*, 7756.
(49) Perdew, J. P.; Burke, K.; Emzerhof, M. *Phys. Rev. Lett*. **1996**, *77*, 3865.
(50) Yourdshahyan, Y.; Rappe, A. M. *J. Chem. Phys*. **2002**, *117*, 825.
(51) Schreiber, F. *Prog. Surf. Sci*. **2000**, *65*, 151.
(52) *CASTEP*, release 4.5; Accelerys Inc.: San Diego, CA, 2001.
(53) Kleinman, L.; Bylander, D. M. *Phys. Rev. Lett.* **1982**, *48*, 1425.
(54) Sierraalta, A.; Ruette, F. *J. Comput. Chem.* **1994**, *15*, 313.
(55) Vyboishchikov, S.; Sierraalta, A.; Frenking, G. *J. Comput. Chem.* **1996**, *18*, 416.
(56) Young, T. *Philos. Trans. R. Soc. London* **1805**, *95*, 65.
(57) Dupre, A. *Theorie Mecanique de la Chaleur*, *Paris*, **1869**.
(58) Campbell, C. T. *Surf. Sci. Rep*. **1997**, *27*, 1.
(59) Sangiorgi, R.; Muolo, M. L.; Chatain, D.; Eustathopoulos, N. *J. Am. Ceram. Soc*. **1988**, *71*, 742.
(60) A factor inversely proportional (See ref 57) to the area per water molecule can convert energies from “per mole” to “per unit area”; however, it is just a constant and therefore it does not matter to the studied correlation.
(61) Ratajczak, H., Orville-Thomas, W. J., Eds. *Molecular Interactions*, *Vol. 1*; John Wiley & Sons: New York, 1980.
(62) Morokuma, H.; Kitaura, K. In *Molecular Interactions*, *Vol. 1*; Ratajczak, H., Orville-Thomas, W. J., Eds. John Wiley & Sons: New York, 1980.
(63) MacDougall, P. J.; Henze, C. E. *Theor. Chem. Acc*. **2001**, *105*, 345.